

# The Physical Origin of the Mass-Size Relation and Its Scatter of Disk Galaxies

Min Du<sup>1,\*</sup>, Hong-Chuan Ma<sup>1</sup>, Wen-Yu Zhong<sup>1</sup>, Luis C. Ho<sup>2,3</sup>, Shihong Liao<sup>4</sup>, and Yingjie Peng<sup>2,3</sup>

<sup>1</sup> Department of Astronomy, Xiamen University, Xiamen, Fujian 361005, China

<sup>2</sup> Kavli Institute for Astronomy and Astrophysics, Peking University, Beijing 100871, China

<sup>3</sup> Department of Astronomy, School of Physics, Peking University, Beijing 100871, China

<sup>4</sup> Key Laboratory for Computational Astrophysics, National Astronomical Observatories, Chinese Academy of Sciences, Beijing 100101, China

March 27, 2024

## ABSTRACT

**Aims.** This study investigates the intricate interplay between internal (natural) and external (nurture) processes in shaping the scaling relationships of specific angular momentum ( $j_*$ ), stellar mass ( $M_*$ ), and size of disk galaxies within the IllustrisTNG simulation.

**Methods.** Utilizing a kinematic decomposition of simulated galaxies, we focus on galaxies with tiny kinematically inferred stellar halos, indicative of weak external influences. The correlation among mass, size, and angular momentum of galaxies is examined by comparing simulations with observations and the theoretical predictions of the exponential hypothesis.

**Results.** Galaxies with tiny stellar halos exhibit a large scatter in the  $j_*$ - $M_*$  relation, which suggests that it is inherently present in their initial conditions. The analysis reveals that the disks of these galaxies adhere to the exponential hypothesis, resulting in a tight fiducial  $j_*$ - $M_*$ -scale length (size) relation that is qualitatively consistent with observations. The inherent scatter in  $j_*$  provides a robust explanation for the mass-size relation and its substantial variability. Notably, galaxies that are moderately influenced by external processes closely adhere to a scaling relation akin to that of galaxies with tiny stellar halos. This result underscores the dominant role of internal processes in shaping the overall  $j_*$ - $M_*$  and mass-size relation, with external effects playing a relatively minor role in disk galaxies. Furthermore, the correlation between galaxy size and the virial radius of the dark matter halo exists but fails to provide strong evidence of the connection between galaxies and their parent dark matter halos.

**Key words.** Galaxy evolution – Galaxy structures – Galaxy stellar disks – Galaxy stellar halos – Astronomical simulations

## 1. Introduction

The size and morphology of galaxies provide valuable insights into the formation of galaxies and the accumulation of stellar mass. In the standard picture of disk galaxy formation (e.g., White & Rees 1978; Fall & Efstathiou 1980), disk galaxies are believed to form as baryons cool inside dark matter haloes, which grow through gravitational instability and acquire angular momentum from cosmological tidal torques (e.g. Hoyle 1951; Peebles 1969; Doroshkevich 1970; White 1984). According to this paradigm, the baryons inherit the same distribution of specific angular momentum as the dark matter, and this conservation is maintained during the cooling process, except when large spheroids form. In this picture, baryonic matter settles into an exponential disk in centrifugal equilibrium. The size of this disk is largely determined by stellar mass  $M_*$  and specific angular momentum  $j_*$ . Analytical models based on these assumptions have been successful in producing disk sizes for a given  $M_*$  that align reasonably well with observations (e.g., Dalcanton et al. 1997; Mo et al. 1998; Dutton et al. 2007; Somerville et al. 2008). The size  $r_e$  of a disk galaxy is proportional to the virial radius  $r_{\text{vir}}$  of its parent dark matter halo with a form as  $r_e \propto \lambda r_{\text{vir}}$ , as presented by the standard framework of Mo et al. (1998). Here the spin parameter  $\lambda = j_h / (\sqrt{2} v_{\text{vir}} r_{\text{vir}})$  is a dimensionless parameter that is often used to characterize the specific angular momentum of dark matter halos  $j_h$ .  $v_{\text{vir}}$  is the virial velocity of the halo.

The debate surrounding the mass and structural assembly of galaxies is still highly contested. Modern advanced cosmological hydrodynamic simulations, e.g., EAGLE simulations (Schaye et al. 2015), IllustrisTNG (TNG hereafter), SIMBA (Davé et al. 2019), and NewHorizon (Dubois et al. 2021), have successfully produced galaxies with realistic morphologies across a wide mass range, thus a powerful tool for gaining profound insights into physical correlations. It is well-established that galaxy sizes are related to both stellar and Active Galactic Nucleus (AGN) feedback (summarized by Somerville & Davé 2015; Naab & Ostriker 2017). Therefore, some previous studies found either no correlation or only a weak correlation between the residual in  $r_e/r_{\text{vir}}$  and the halo spin parameter (Teklu et al. 2015; Zavala et al. 2016; Zjupa & Springel 2017; Desmond et al. 2017). However, there are also clear indications that the properties of galaxies are heavily influenced by their parent dark matter halos in numerous aspects. For instance, Zavala et al. (2016) and Lagos et al. (2017) identified a noteworthy link between the specific angular momentum evolution of the dark matter and baryonic components of galaxies in EAGLE simulations. Yang et al. (2023) demonstrated that disk-dominated galaxies selected via kinematics in TNG and AURIGA (Grand et al. 2017) reproduce a correlation between galaxy sizes and the spin parameters of their dark matter haloes. Similarly, Desmond et al. (2017) found a weak correlation between galaxy size and the host halo spin parameter in the EAGLE simulation. Liao et al. (2019) uncovered a strong correlation between sizes and host halo spin parameters

\* E-mail: dumin@xmu.edu.cn

for field dwarf galaxies in the AURIGA simulation. Zanisi et al. (2020) contended that the scatter in the galaxy-halo size relation for late-type galaxies could be explained by the scatter in stellar angular momentum, rather than the halo spin parameter. Jiang et al. (2019) also identified a weak correlation between size and spin in the VELA and NIHAO zoom-in simulations, but instead found a significant correlation between size and NFW halo concentration.

Especially, Du et al. (2022) showed that the TNG simulations (Marinacci et al. 2018; Nelson et al. 2018, 2019; Naiman et al. 2018; Pillepich et al. 2018, 2019; Springel et al. 2018) have achieved significant success in replicating a  $j_\star \propto M_\star^{0.55}$  relationship consistent with observations (see also e.g., Rodriguez-Gomez et al. 2022). Upon closer investigation of the disk galaxies from TNG, it was revealed that this scaling relation arises as a consequence of three physically meaningful scaling relations involving  $j_\star$ ,  $M_\star$ , total mass  $M_{\text{tot}}$ , and total specific angular momentum  $j_{\text{tot}}$ : (a) the  $j_{\text{tot}} \propto M_{\text{tot}}^{0.81}$  relation deviates notably from the tidal torque theory’s prediction of  $j_{\text{tot}} \propto M_{\text{tot}}^{2/3}$ ; (b) the stellar-to-halo mass ratio consistently increases in log-log space according to  $M_{\text{tot}} \propto M_\star^{0.67}$ ; (c) angular momentum is approximately conserved (with a certain factor) during galaxy formation, i.e.,  $j_{\text{tot}} \propto j_\star$ . Du et al. (2022) suggest that the assembly of disk galaxies in the TNG simulation follows a consistent framework akin to that proposed by Mo et al. (1998), but some adjustments, potentially attributable to baryonic processes, should be considered for a more precise understanding.

It is crucial to disentangle the influence of external factors to comprehend the formation of galaxies in terms of their properties and structure. Indeed, both galaxy size and mass growth are significantly influenced by external processes, especially major mergers. Specifically, gas-poor mergers tend to increase galaxy size, whereas gas-rich mergers lead to a decrease in size (Covington et al. 2008; Naab et al. 2009; Hopkins et al. 2009; Covington et al. 2011; Oser et al. 2012). Consequently, the variation in galaxy size for these entities would be expected to correlate with both the frequency of mergers experienced by a galaxy and the gas content of those mergers, i.e., nurture. Covington et al. (2008, 2011) and Porter et al. (2014) have presented findings on the size evolution of bulge-dominated galaxies by incorporating the size growth observed in binary merger simulations into a semi-analytic model, exhibiting overall good agreement with observational data (see also Shankar et al. 2013). Romanowsky & Fall (2012) argued that the Hubble sequence of galaxy morphologies is a sequence of increasing angular momentum at any fixed mass. Obreschkow & Glazebrook (2014) introduce the  $j_\star$ - $M_\star$ -morphology relation wherein morphology is quantified by the mass fraction of bulges. Rodriguez-Gomez et al. (2022) identified a  $j_\star$ - $M_\star$ -morphology relation in TNG, albeit with a notable degree of scatter. This picture suggests galaxy mergers, particularly “dry” major mergers, can give rise to the parallel trajectory observed in the  $j_\star$ - $M_\star$  diagram by effectively disrupting the disk structures of galaxies. As a consequence, earlier-type galaxies generally exhibit weaker rotational characteristics and have massive bulges in morphology.

Moreover, extensive research indicates that the present-day profile of a galactic disk is not primarily determined by the initial conditions, even in the absence of mergers. Simulations pertaining to the formation of disk galaxies consistently reveal that the distribution of stellar birth radii often exhibits substantial deviations from an exponential profile (Debatista et al. 2006; Roškar et al. 2008, 2012; Minchev et al. 2012; Berrier & Sellwood 2015; Herpich et al. 2015). This deviation occurs because stars do not

remain confined to their original orbits, but exert minimal impact on the overall angular momentum of the galaxy disk. Both analytical arguments and numerical experiments have demonstrated that the angular momenta of individual disk particles are influenced by transient non-axisymmetric perturbations, such as spiral arms and bars, leading to a process commonly referred to as “churning” or “shuffling” (e.g., Sellwood 2014, and references therein). This phenomenon is commonly known as radial migration which can significantly change the profile of a galactic disk.

Isolating the internal and external processes can be a key to uncovering the underlying mechanisms of the assembly of galaxies. This duality is underscored in studies of Du et al. (2020) and Du et al. (2021), where the authors employ a fully automatic kinematical method to decompose the kinematic intrinsic structures of TNG galaxies (Du et al. 2019). The mass ratio of kinematically derived stellar halos is sensitive to external impacts and thus can be used to quantify the effect of external processes in galaxies (Section 2). The conceptual significance of the “nature-nurture” framework, within the context of internal versus external factors, is illustrated in Section 2.2. Galaxies that have experienced minimal external effects give the fiducial  $j_\star$ - $M_\star$ -size relation, which is detailed in Sections 3 and 4. This scaling relation is primarily governed by universal and natural physical processes, while nurture plays a minor role. In Section 5, we summarize the result.

## 2. Sample selection and data extraction

### 2.1. The IllustrisTNG Simulation

The TNG Project is a suite of cosmological simulations run with the moving-mesh code AREPO (Springel 2010; Pakmor et al. 2011, 2016) that utilized gravo-magnetohydrodynamics and incorporates a comprehensive galaxy model (Weinberger et al. 2017; Pillepich et al. 2018). The TNG50-1 run within the TNG suite has the highest resolution, consisting of  $2 \times 2160^3$  initial resolution elements in a comoving box of approximately 50 Mpc. This corresponds to a baryon mass resolution of  $8.5 \times 10^4 M_\odot$  and a gravitational softening length for stars of about 0.3 kpc at redshift  $z = 0$ . Dark matter particles are resolved with a mass of  $4.5 \times 10^5 M_\odot$ , while the minimum gas softening length reaches 74 comoving parsecs. These resolutions enable the accurate reproduction of the overall kinematic properties of galaxies with stellar masses greater than or equal to  $10^9 M_\odot$  (Pillepich et al. 2019).

The identification and characterization of galaxies within the simulations are performed using the friends-of-friends (Davis et al. 1985) and SUBFIND algorithms (Springel et al. 2001). Resolution elements including gas, stars, dark matter, and black holes that belong to an individual galaxy are gravitationally bound to its host subhalo. All galaxies in our sample are rotated to the face-on view based on the stellar angular momentum to measure properties accurately.

To determine the positions of galaxies, we employ a centering method that places them at the location corresponding to the minimum gravitational potential energy in all measurements. The bulk velocity of all particles is subtracted. All quantities presented in this paper are computed using the full complement of particles associated with galaxies and subhalos, encompassing all gravitationally bound particles identified through the SUBFIND algorithm. We refrain from imposing any constraints on the radial extent of galaxies when deriving their comprehensive properties. The units of length,  $j$ , and mass use kpc, kpc-km

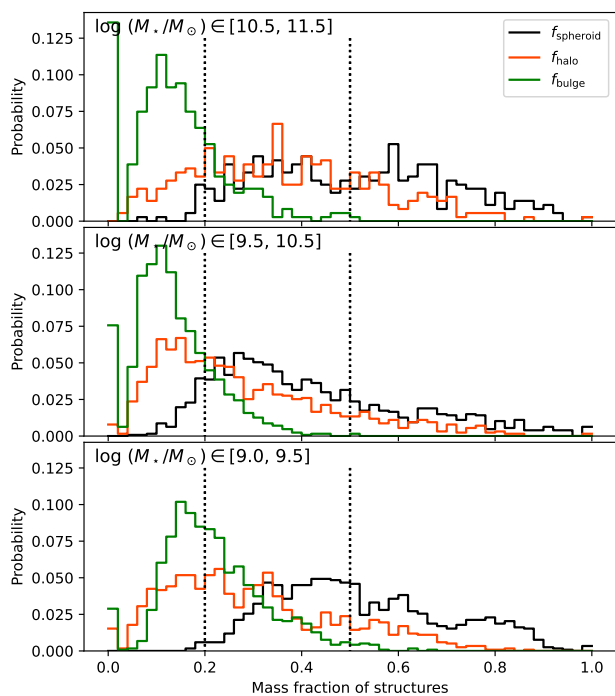


**Fig. 1.** The distribution of the mass fraction of kinematic structures in TNG50 galaxies. The bar heights are normalized their sum to 1. Then we classify galaxies into tiny-halo galaxies, halo-subdominated galaxies, and halo-dominated galaxies by  $f_{\text{halo}} \leq 0.2$ ,  $0.2 < f_{\text{halo}} \leq 0.5$ , and  $f_{\text{halo}} > 0.5$ , respectively. The criterion  $f_{\text{halo}} = 0.2$  and  $0.5$  are marked by the black vertical lines. The mass fraction of spheroids  $f_{\text{spheroid}}$  is equal to  $f_{\text{bulge}} + f_{\text{halo}}$ . From top to bottom, we show the galaxies with stellar mass  $\log(M_*/M_\odot) \in [10^9, 10^{11.5}]$ . The galaxies with  $\log(M_*/M_\odot) \in [9.5, 10.5]$  are the most representative sample.

$s^{-1}$ , and  $M_\odot$ , respectively, over the paper. ‘log’ always represents the logarithm with base 10.

## 2.2. Physical meaning of kinematic structures: data extraction and galaxy classification

We recently developed an automated method called auto-GMM to efficiently decompose the structures of simulated galaxies based on their kinematic phase space properties (Du et al. 2019, 2020). This method used the GaussianMixture Module (GMM) of the Python scikit-learn package to cluster the three-dimensional phase space of dimensional parameters that quantify circularity, binding energy, and non-azimuthal angular momentum (Doménech-Moral et al. 2012) into distinct structures. Such kind of kinematic method has become a standard way to decompose galaxies accurately (see similar attempts in Obreja et al. 2018; Zana et al. 2022; Proctor et al. 2024). We successfully identified cold disk, warm disk, bulge, and stellar halo structures of TNG galaxies using auto-GMM (Du et al. 2020). The overall disk and spheroidal structures are obtained by summing the stars from the cold+warm disks and the bulge+stellar halo, respectively. Notably, stars within kinematically derived disks are predominantly characterized by strong rotation, exhibiting a mass-weighted average circularity  $\langle j_z/j_c \rangle > 0.5$ , where  $j_z$  and  $j_c$  are the azimuthal and circular angular momentum, respectively. Conversely, the kinematically derived stellar halos share a similar weak rotation ( $\langle j_z/j_c \rangle < 0.5$ ) with bulges but possess looser binding stars than bulges. It’s important to

emphasize that this decomposition method does not assume that the disk of a galaxy follows an exponential profile, nor does it presuppose that the bulge follows a Sérsic profile.

In Du et al. (2021), we propose the “nature-nurture” picture to understand the structures of galaxies and their evolution. In this paper, “nature” is equivalent to internal processes, while “nurture” is equivalent to external processes. By successfully identifying kinematic structures within galaxies, it becomes possible to establish connections between these structures and either nature (internal) or nurture (external) physical processes. The early phase at redshifts  $z > 2$ , characterized by chaotic physical processes and gas accretion in the host dark matter halo and protogalaxy, is regarded as the one aspect of galaxy nature. In the later phase, there is no doubt that long-term evolution belongs to nature in the absence of significant mergers. Consequently, the nature of galaxies substantially contributes to the formation of both kinematic bulges and disk structures, as demonstrated by Du et al. (2021). In contrast, only kinematic stellar halos are strongly linked to external events, primarily mergers but not exclusively, representing the “nurture” aspect.

In this study, our primary focus is to elucidate the influence of internal and external processes on the scaling relations of  $j_\star$ - $M_\star$  and the size of galaxies from TNG50. We utilize galaxies within the stellar mass range of  $10^9 - 10^{11.5} M_\odot$  from the TNG50-1 simulation. Figure 1 presents the distribution of the mass fractions of kinematic structures in three stellar mass ranges from top to bottom, as detailed in Du et al. (2021)<sup>1</sup>. We proceeded to categorize galaxies into three groups based on their stellar halo mass fractions  $f_{\text{halo}}$ , as follows:

- *Tiny-halo galaxies*:  $f_{\text{halo}} \leq 0.2$  select 997 galaxies. These galaxies are robustly classified as disk galaxies in terms of morphology and can be considered to have formed via internal processes, largely unaffected by mergers and other environmental factors. They serve as the physical basis for the fiducial scaling relations.
- *Halo-subdominated galaxies*:  $0.2 < f_{\text{halo}} \leq 0.5$  select 1369 galaxies. The morphological classification of such galaxies is challenging. The existence of a massive stellar halo is a sign that such a galaxy has experienced somewhat external effects. It thus may lead to a scatter in any fiducial scaling relation originating from internal processes.
- *Halo-dominated galaxies*:  $f_{\text{halo}} > 0.5$  select 442 galaxies, indicating elliptical galaxy morphology. For these galaxies, any fiducial scaling relation resulting from internal processes may have been disrupted or substantially altered due to the pronounced influence of external processes.

In comparison with the ex-situ mass fraction measured in Rodriguez-Gomez et al. (2015), the use of  $f_{\text{halo}}$  is more convenient, as it eliminates the need to account for variations in the strength, orbits, and frequency of mergers and close tidal interactions. The mass fraction of spheroids  $f_{\text{spheroid}}$  in each galaxy can be computed simply as  $f_{\text{bulge}} + f_{\text{halo}}$ .

## 3. The fiducial $j_\star$ - $M_\star$ - $h_R$ plane of bulge/disk-dominated galaxies from their exponential nature

It is well known that more massive galaxies have larger sizes, although the scatter is large at given  $M_\star$  (e.g., Shen et al. 2003;

<sup>1</sup> The data of kinematic structures in TNG galaxies are publicly accessible at <https://www.tng-project.org/data/docs/specifications/#sec5m>

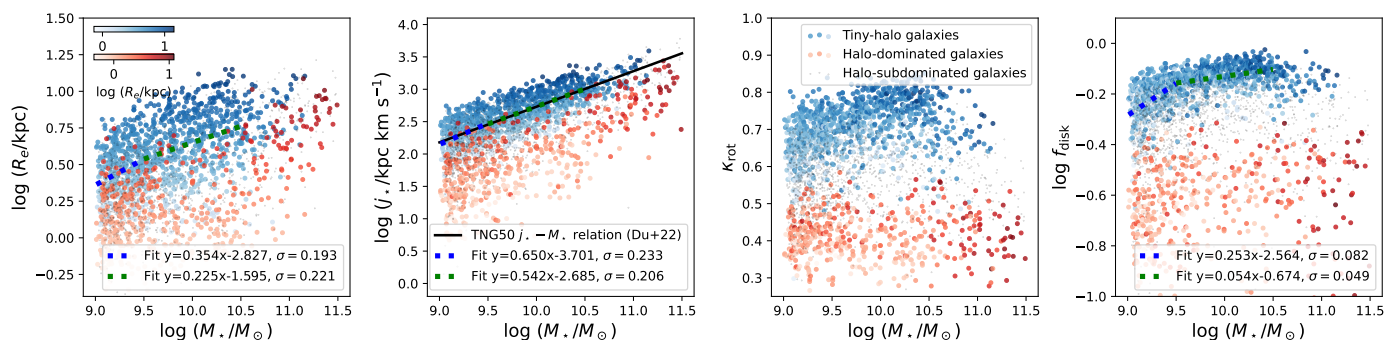


**Fig. 2.** The scaling relations of tiny-halo (blue dots), halo-subdominated (gray dots), and halo-dominated (red dots) galaxies. From left to right, we show  $M_\star$ - $R_e$  relation,  $j_\star$ - $M_\star$  relation, rotation  $\kappa_{\text{rot}}$ , and the mass fraction of disk structures  $f_{\text{disk}}$ . The deepness of red and blue colors represents the  $\log(R_e/\text{kpc})$  in all panels, showing that larger galaxies have relatively larger  $j_\star$  for a given stellar mass. The green triangle symbols show the observational result from Mancera Piña et al. (2021). We perform the linear fitting for galaxies in two mass ranges  $\log(M_\star/M_\odot) \in [9.5, 11.5]$  (green dotted lines) and  $[9., 9.5]$  (blue dotted lines), respectively. The  $j_\star$ - $M_\star$  relation of disk galaxies from Du et al. (2022) is overlaid in black in the second panel.

Fernández Lorenzo et al. 2013; Lange et al. 2015; Muñoz-Mateos et al. 2015). TNG has successfully reproduced the relation between stellar mass and half-mass radius  $R_e$  within observational uncertainties (e.g., Genel et al. 2018; Huertas-Company et al. 2019; Rodríguez-Gomez et al. 2019, see also the left-most panel of Figure 2). But the substantial scatter in galaxy sizes, ranging from 1 kpc to more than 10 kpc, and in  $j_\star$  (Du et al. 2022; Fall & Rodríguez-Gomez 2023) continue to pose a perplexing challenge. In this study, we isolate the influence of internal processes on the mass-size relation and  $j_\star$  by selecting the tiny-halo galaxies. The effect of nurture then is shown by comparing halo-subdominated and halo-dominated galaxies with their counterparts with tiny stellar halos.

### 3.1. The large scatter of the $j_\star$ - $M_\star$ relation

Conducting a comparative study is crucial to differentiate between the effects of internal and external processes on galaxy evolution and the large scatter of the  $j_\star$ - $M_\star$  relation. In the second panel of Figure 2, we show the  $j_\star$ - $M_\star$  relation for the three types of galaxies defined in Section 2, e.g., tiny-halo galaxies (blue dots), halo-subdominated galaxies (gray dots), and halo-dominated galaxies (red dots). Tiny-halo galaxies in the absence of mergers exhibit the almost exactly same  $j_\star$ - $M_\star$  relation (the blue and green dotted lines fitted in different mass ranges) to disk galaxies selected based on the relative importance of cylindrical rotations ( $\kappa_{\text{rot}} \geq 0.5$ ) as described in Du et al. (2022), corresponding to the black solid line. Specifically, these galaxies follow a scaling relation of  $j_\star \propto M_\star^{0.55}$ . This finding suggests that the wide scatter observed around the  $j_\star \propto M_\star^{0.55}$  relation exists regardless of whether external processes have played a significant role in their evolution. Moreover, it is evident that halo-subdominated and halo-dominated galaxies generally possess smaller  $j_\star$  values for a given  $M_\star$ . It is not surprising that mergers induce the increase of mass as well as the decrease of angular momentum via destroying disky structures.

The extensive scatter observed in the  $j_\star$ - $M_\star$  relation of tiny-halo galaxies exhibits a distinct correlation with the galaxy size, as indicated by the depth of the blue color in the plot. Furthermore, our analysis does not reveal a significant correlation between rotation and  $R_e$  in these galaxies, as demonstrated in the third and fourth panels of Figure 2. The substantial scatter in the  $j_\star$ - $M_\star$  relation primarily stems from the significant variation in

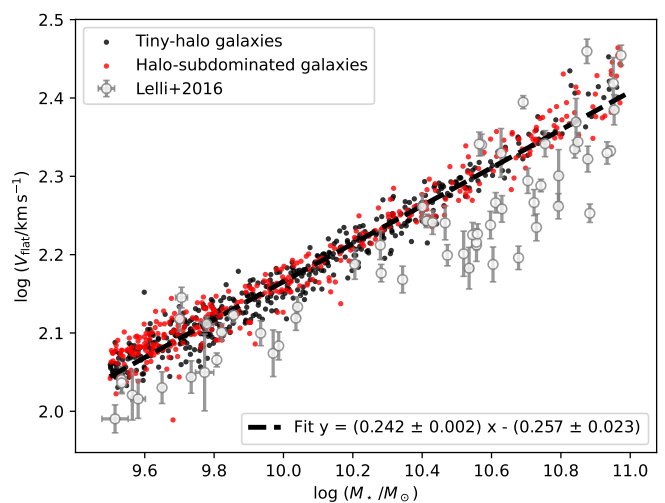


**Fig. 3.** The Tully-Fisher relation of galaxies in TNG (black and red dots) and observations. The  $v_{\text{flat}}$  of TNG galaxies is measured by averaging the flat part ( $0.05 - 0.2r_{\text{vir}}$ ) of the rotation curve. The observations are adopted from Lelli et al. (2016) assuming the mass-to-light ratio  $\Gamma = 0.5M_\odot/L_\odot$  based on the IMF suggested by Kroupa et al. (2001).

galaxy size, driven by internal processes, as elucidated in Sections 3.2 and 4. It is not surprising that both halo-subdominated and halo-dominated galaxies exhibit a clear deviation towards lower  $j_\star$  compared to the  $j_\star$ - $M_\star$  relation of tiny-halo galaxies, which is consistent with the prediction of the so-called  $j_\star$ - $M_\star$ -morphology relation (Sweet et al. 2018; Obreschkow & Glazebrook 2014; Rodríguez-Gomez et al. 2022). This divergence is linked to their noticeably weaker rotation shown in the third and fourth panels. But the scatter of  $j_\star$  from nature plays a more important role. We thus can conclude that a pronounced scatter in the  $j_\star$ - $M_\star$  relation is inherently present in the initial conditions of galaxies, shaping the observed  $j_\star$ - $M_\star$  relation and mass-size relation in the local Universe. On the other hand, external influences induce a systematic offset, further contributing to this inherent variation.

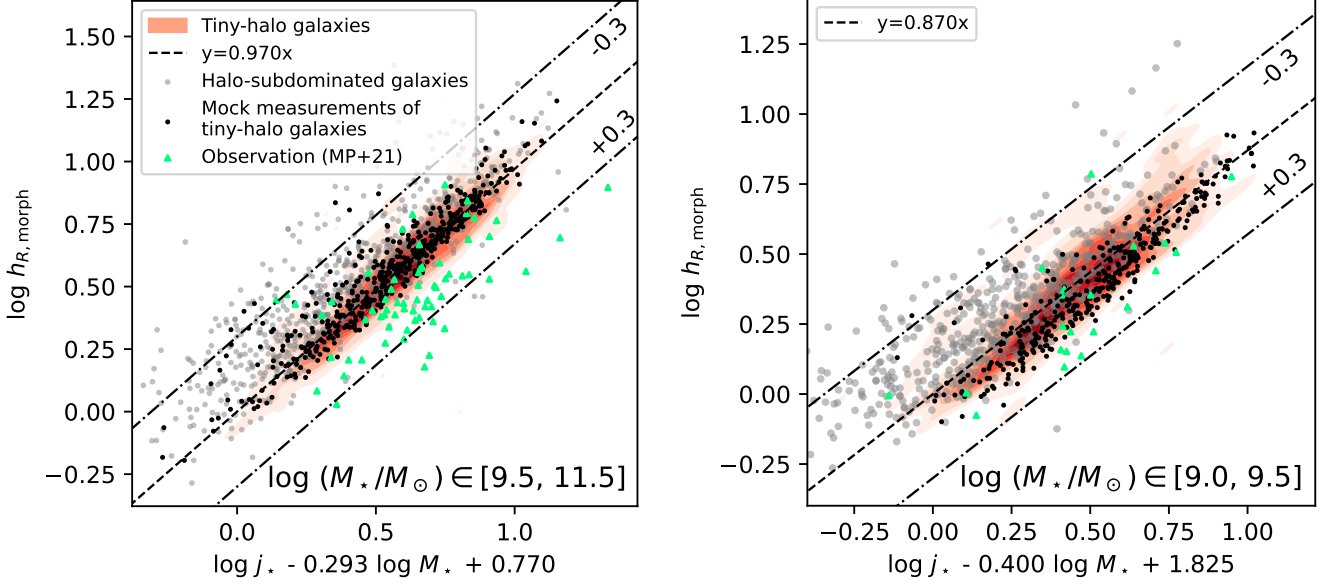


**Fig. 4.** The  $j_*$ - $M_*$ - $h_{R,\text{morph}}$  relation comparing simulations with observations. The units of  $h_{R,\text{morph}}$ ,  $j_*$ , and  $M_*$  use kpc, kpc-km/s, and  $M_\odot$ , respectively. The left and right panels show galaxies in two mass ranges  $\log(M_*/M_\odot) \in [9.5, 11.5]$  and  $\in [9.0, 9.5]$ . The fiducial  $j_*$ - $M_*$ - $h_{R,\text{morph}}$  relation of tiny-halo galaxies, where  $h_{R,\text{morph}}$  represents the scale length of the disk component defined by morphology, is visualized using kernel density estimation (KDE) map. For convenience, we adjust the surface fitting to align with  $y = x$ . We perform mock measurements of tiny-halo galaxies based on Equation (2) (black dots). The gray points show the halo-subdominated galaxies for comparison. The observational data points of disk galaxies from Mancera Piña et al. (2021) are represented by green triangles. The dot-dashed lines represent the cases exhibiting offsets of  $\pm 0.3$  dex.

### 3.2. The fiducial $j_*$ - $M_*$ - $h_R$ relation in nature satisfying the exponential hypothesis

In a realistic scenario of the exponential hypothesis, galaxies consist of both spheroidal and disk components. The angular momentum of a galaxy is largely determined by the mass fraction of its disk components, denoted as  $f_{\text{disk}}$ , as spheroidal components exhibit little or no rotation. Here a disk structure includes thin (cold) and thick (warm) disk components. We then have

$$\begin{aligned} j_{\star,\text{theory}} &= f_{\text{disk}} j_{\text{disk}} \\ &= \frac{1}{M_\star} \int 2\pi R^2 \Sigma_{\text{disk}}(R) v_\phi(R) dR. \end{aligned} \quad (1)$$

$v_\phi$  and  $\Sigma_{\text{disk}}$  are the cylindrical rotation velocity and surface density at cylindrical radius  $R$ , respectively. Exponential disks exhibit a simple surface density profile described as  $\Sigma_{\text{disk}} = \Sigma_{0,\text{disk}} \exp(-R/h_{R,\text{theory}})$ . The central surface density  $\Sigma_{0,\text{disk}}$  can be expressed as  $f_{\text{disk}} M_\star / (2\pi h_{R,\text{theory}}^2)$ .  $\int R^2 \exp(-R/h_{R,\text{theory}}) dR$  integrates from 0 to infinity resulting in  $2h_{R,\text{theory}}^3$ . The accuracy of estimating  $j_{\star,\text{theory}}$  using Equation (1) hinges on the precise characterization of disk structures by  $h_{R,\text{theory}}$ ,  $f_{\text{disk}}$ , and their rotation curves. We define the factor  $\epsilon = \langle v_\phi / v_{\text{flat}} \rangle$  to quantify the deviation of  $v_\phi$  from the flat rotation curve with a velocity  $v_{\text{flat}}$ .  $\epsilon$  thus has a similar physical meaning to the circularity  $\langle j_z / j_c \rangle$ . Through a simple derivation, Equation (1) gives

$$\begin{aligned} j_{\star,\text{theory}} &= \frac{2\pi\epsilon\Sigma_{0,\text{disk}}v_{\text{flat}}}{M_\star} \int R^2 e^{-R/h_{R,\text{theory}}} dR \\ &= 2\epsilon f_{\text{disk}} v_{\text{flat}} h_{R,\text{theory}} \end{aligned} \quad (2)$$

This equation is physically robust in cases where galaxies satisfy the exponential hypothesis. It thus has been commonly used as

an approximation of  $j_*$  (e.g., Fall 1983; Mo et al. 1998), via measuring  $f_{\text{disk}}$  in morphology and making corrections by adding asymmetric drift.

It should be noted that Equation (2) holds when we can accurately measure the mass fraction of disks that possess strong rotation and conform to an exponential distribution. Moreover, the TF relation  $M_\star \propto v_{\text{flat}}^\alpha$  is generally tightly satisfied where the gaseous component is negligible in the local Universe. Observations give a consistent result in previous studies that  $\alpha$  varies between 3 and 4 (e.g., Noordermeer & Verheijen 2007; Avila-Reese et al. 2008; Gurovich et al. 2010; Zaritsky et al. 2014; Bradford et al. 2016; Papastergis et al. 2016; Lelli et al. 2019). The TF relation we measured in TNG50 tiny-halo galaxies (black dots in Figure 3) gives  $\log(v_{\text{flat}}/\text{km s}^{-1}) = (0.242 \pm 0.002) \log(M_\star/M_\odot) - (0.257 \pm 0.023)$  that is consistent with the observation from Lelli et al. (2016) (gray dots with error bars). We then have the fiducial  $j_*$ - $M_*$ -size relation based on the theory of the exponential hypothesis

$$\begin{aligned} \log(h_{R,\text{theory}}/\text{kpc}) &\simeq \\ \log(j_{\star,\text{theory}}/\text{kpc km s}^{-1}) - 0.24 \log(M_\star/M_\odot) + C_0. \end{aligned} \quad (3)$$

The constant part  $C_0$  is  $-\log(2\epsilon f_{\text{disk}}) - C_{\text{TF}}$  where  $C_{\text{TF}} = -0.26$  is the zero point of the TF relation.  $C_0$  is nearly constant around 0.3 estimated by  $f_{\text{disk}} \sim 0.7$  and  $\epsilon \sim 0.7$ . After considering the correction from  $f_{\text{disk}}$ , the right-most panel of Figure 2 gives  $\log f_{\text{disk}} = 0.054 \log(M_\star/M_\odot) - 0.674$ . Then we have

$$\begin{aligned} \log(h_{R,\text{theory}}/\text{kpc}) &\simeq \\ \log(j_{\star,\text{theory}}/\text{kpc km s}^{-1}) - 0.29 \log(M_\star/M_\odot) + C_1 \end{aligned} \quad (4)$$

where  $C_1 = -\log(2\epsilon) + 0.94$ .  $\epsilon$  varies in the range of 0.85 – 1.0 and 0.5 – 0.85 for cold and warm disks, respectively, defined by

the kinematical method in Du et al. (2020). It is roughly constant around 0.7 estimated by the relative mass fraction of cold and warm disks. A dynamically hotter disk has a smaller  $\epsilon$ . Then  $C_1$  is about 0.79. The upper and lower limits can be 0.94 and 0.64 in the case of  $\epsilon = 0.5$  and  $\epsilon = 1$ , respectively. Such a theoretical  $j_\star$ - $M_\star$ - $h_R$  relation relies on the assumption that disks accurately satisfy the exponential profile and bulges have zero rotation. It is worth emphasizing that the correction of  $\log f_{\text{disk}}$  is non-negligible, which may induce a deviation of  $C_1 - C_0 \sim 0.5$  dex when the difference in the factor of the  $\log M_\star$  is ignored.

We examine whether tiny-halo galaxies in TNG50 obey the theoretical  $j_\star$ - $M_\star$ - $h_R$  relation (Equation (4)). We first perform a surface fitting in the 3-dimensional (3D) space using  $j_\star$ ,  $M_\star$ , and  $h_{R,\text{morph}}$  for tiny-halo galaxies in two mass ranges  $\log(M_\star/M_\odot) \in [9, 9.5]$  and  $\in [9.5, 11.5]$ . Figure 4 then shows the fitting results in a 2D way which is convenient to compare with Equation (4).  $h_{R,\text{morph}}$  is extracted using a 1D two-component (Sérsic bulge + exponential disk) morphological decomposition that has been widely used in observations. We here use a 1D bulge-disk decomposition to simplify the analysis, as the face-on surface density map of galaxies is exactly known in simulations.

The fitting result of the fiducial  $j_\star$ - $M_\star$ - $h_R$  relation of tiny-halo galaxies with  $\log(M_\star/M_\odot) \in [9.5, 11.5]$  in TNG50 simulation gives

$$\log h_{R,\text{morph}} = (0.970 \pm 0.020) [\log j_\star - (0.293 \pm 0.015) \log M_\star + (0.770 \pm 0.123)] \quad (5)$$

Where the units of  $h_{R,\text{morph}}$ ,  $j_\star$ , and  $M_\star$  use kpc, kpc-km/s, and  $M_\odot$ , respectively. The left and right parts of this equation are used as the  $y$  and  $x$  axes, respectively, in Figure 4. The fitting result matches Equation (4) perfectly, suggesting that galaxies evolve in a natural way obeying the exponential hypothesis. It is worth emphasizing that the kinematic disk structures indeed show some noticeable deviations from simple exponential profiles (see Figure 12 in Du et al. 2022), while the exponential hypothesis is still valid to explain the overall properties. This result is not sensitive to stellar mass for massive galaxies but has a clear deviation in less-massive galaxies. The right panel of Figure 4 gives the fiducial  $j_\star$ - $M_\star$ - $h_R$  relation of dwarf galaxies with  $\log(M_\star/M_\odot) \in [9, 9.5]$

$$\log h_{R,\text{morph}} = (0.870 \pm 0.024) [\log j_\star - (0.400 \pm 0.043) \log M_\star + (1.825 \pm 0.387)]. \quad (6)$$

The deviation with respect to the more massive galaxies is largely due to that  $\log f_{\text{disk}}$  (blue dashed line) has a steeper slope and a smaller intercept, as shown in the right-most panel of Figure 2.

Moreover, the halo-subdominated galaxies (gray dots) exhibit a similar  $j_\star$ - $M_\star$ - $h_R$  relation, albeit with a noticeable degree of scatter. These galaxies clearly deviate towards the left side in comparison to the fiducial  $j_\star$ - $M_\star$ - $h_R$  relation depicted in Figure 4. This deviation is likely attributed to the reduced  $j_\star$  from external influences.

In summary, disk structures of TNG galaxies do conform to the exponential hypothesis. The significant scatter in the  $j_\star$ - $M_\star$  relation, as seen in Figure 2, which is inherent in protogalaxies or their host dark matter halos, effectively explains the underlying physical basis for the fiducial  $j_\star$ - $M_\star$ - $h_R$  relation. Consequently, this scatter results in a wide range of galaxy sizes, indicating that the evolution of these galaxies has only been minimally impacted by external influences. External factors play a relatively minor role in shaping the overall mass-size and  $j_\star$ - $M_\star$  scaling relationships in disk galaxies. Moreover, this result suggests that

the effect of stellar migrations (e.g. Debattista et al. 2006; Roškar et al. 2012; Berrier & Sellwood 2015; Herpich et al. 2015) also has a minor effect on the overall properties of disk galaxies.

### 3.3. The deviation of the $j_\star$ - $M_\star$ - $h_R$ relation between the TNG50 simulation and observations

The fiducial  $j_\star$ - $M_\star$ - $h_R$  relation on the basis of the exponential hypothesis provides a reference point for galaxies that are primarily rotation-dominated. It provides valuable constraints on the physical model to explain the galaxy's size. In Figure 4, we compare the observational data with the fiducial  $j_\star$ - $M_\star$ - $h_R$  relation derived from TNG50. The observational data of  $j_\star$  utilized in this study are sourced from Mancera Piña et al. (2021) (green triangles). It is worth emphasizing that all observed galaxies here are in close proximity, allowing for relatively reliable measurements of  $M_\star$  and  $h_{R,\text{morph}}$  enabling a meaningful comparison. The estimation of the mass fraction and  $h_{R,\text{morph}}$  of disks is based on 2D bulge-disk decomposition conducted by Fisher & Drory (2008). This decomposition combines high-resolution Hubble Space Telescope imaging with wide-field ground-based imaging, which helps to minimize uncertainties of  $h_{R,\text{morph}}$  and  $f_{\text{disk}}$ .

Galaxies in TNG50 follow a similar trend to those in observations. But there is indeed a notable discrepancy between the observed galaxies of Mancera Piña et al. (2021) and the galaxies in TNG50, as illustrated in the left panel of Figure 4. This discrepancy is smaller in less massive galaxies, as seen in the right panel. It is evident that many galaxies exhibit an offset of approximately  $> 0.2$  dex to the right of the fiducial  $j_\star$ - $M_\star$ - $h_R$  relation. We first investigate the uncertainty of observations to figure out the potential source of the observed offset. The determination of  $j_\star$  in Mancera Piña et al. (2021) involves measuring the rotation curve from gas after applying a stellar-asymmetric drift correction. Part of the measurements of  $j_\star$  (e.g., Romanowsky & Fall 2012) employs slit spectroscopy of both starlight and ionized gas. According to Sweet et al. (2018), the typical uncertainty of  $j_\star$  is given by  $|\Delta j_\star|/j_\star = 0.05 - 0.1$ , reaching a maximum of 0.32 ( $\sim 0.15$  dex) for the data from Romanowsky & Fall (2012). Moreover, the uncertainty of  $M_\star$  is about 0.2 dex estimated by the uncertainty of the mass-to-light ratio adopting a factor of  $\sim 1.5$ . To estimate the overall uncertainty of  $\log j_\star - 0.3 \log M_\star$ , we can use the formula  $\sqrt{0.15^2 + (0.3 \times 0.2)^2} \approx 0.16$ . This uncertainty can partially explain the inconsistency between the observational results using Equation (2) and simulations.

To quantify any potential uncertainty in the measurement of  $j_\star$ , we perform mock measurements based on Equation (2) (black dots in Figure 4). The  $v_{\text{flat}}$  is measured by the average value of the flat part of the outer edge ( $0.05 - 0.2r_{\text{vir}}$ ) of a rotating curve. We do not make any asymmetric drift correction which will only lead to a negligible offset toward the left side. It thus cannot explain the deviation between observations and TNG simulations. We have confirmed that halo-subdominated galaxies measured using Equation (2) follow a similar  $j_\star$ - $M_\star$ - $h_R$  relation. It is likely because of the fact that the transformation from disks to stellar halos due to mergers generally induces a minor change on both  $v_{\text{flat}}$  and  $h_{R,\text{morph}}$  measured in morphological decomposition. It is clear that halo-subdominated galaxies (red dots) follow a similar TF relation to tiny-halo galaxies (black dots), as shown in Figure 3. Thus,  $j_\star$  of halo-subdominated galaxies are likely to be significantly overestimated using this method, while it will not affect our results in this study.

The observation may not be able to reflect the physics due to poor statistics and large uncertainty. The 3D surface fitting of observational data from Mancera Piña et al. (2021) gives

$$\log h_{R,\text{morph}} = (0.028 \pm 0.089) \log j_\star + (0.345 \pm 0.130) \log M_\star - (0.844 \pm 0.661). \quad (7)$$

This result suggests that  $h_{R,\text{morph}} \propto M_\star^{1/3}$ , which is nearly independent of  $j_\star$ . The strong correlation that implies  $h_{R,\text{morph}} \propto j_\star$  in the fiducial  $j_\star$ - $M_\star$ - $h_R$  relation disappears when only the observational data is considered. However, there is indeed a substantial uncertainty  $\pm 0.661$  dex in the constant part on the right side of Equation (7), indicating that no satisfactory 3D fitting results can be obtained. Moreover, it is worth mentioning that the deviation between simulations and an integral field spectroscopic (IFS) measurement (Sweet et al. 2018) is even larger. Obreschkow & Glazebrook (2014) have already noticed that  $j_\star$  measured by Equation (2) have systematic variations in comparison to the IFS observations. Many observational issues should be examined in detail. We thus do not compare with the result of IFS measurement in this work. Consequently, we still cannot reach a robust conclusion due to the poor statistics and large uncertainty of the observational data.

### 3.4. No strong evidence of incorrect galaxy properties in IllustrisTNG simulations

In the previous section, we demonstrated that the disparity between simulations and observations is predominantly due to measurement uncertainties. As of now, we cannot rule out the possibility that this inconsistency is a result of errors in the simulated galaxy properties generated by the IllustrisTNG simulations. Generating galaxies with a faster flat rotation curve, a smaller disk size, or a larger mass fraction of disk structures in simulations may solve its inconsistency with observations. There is no clear inconsistency in the TF relation, as shown in Figure 3. Though the observational findings by Lelli et al. (2016) (represented by open dots with error bars) are marginally lower compared to the disk galaxies in the TNG50 simulation, this small discrepancy only accounts for a negligible 0.05 dex deviation in the fiducial  $j_\star$ - $M_\star$ - $h_R$  relation. In this section, we further delve into the specific properties of disk galaxies in TNG50 to elucidate the discrepancies in the  $j_\star$ - $M_\star$ - $h_R$  relation observed.

In Figure 5, we show the mass- $h_R$  relation, comparing the tiny-halo galaxies from TNG50 (represented by blue shaded regions) with those observed (triangles). Additionally, we overlay the late-type galaxies from the SDSS DR7 dataset in black. The selection criterion for late-type galaxies is based on a color threshold of  $g - r < 0.7$ , as suggested by Blanton et al. (2003). We adopt the scale length approximated by Simard et al. (2011) and the stellar mass provided by Mendel et al. (2014). It is evident that galaxies in SDSS observations (black histogram and shaded regions) demonstrate a consistent trend with galaxies in TNG50 simulations (blue histogram and shaded regions). The galaxies utilized in Mancera Piña et al. (2021) include a group of compact massive galaxies as we can see by comparing the green with the black and blue histograms on the right side of Figure 5. Such galaxies generally have stellar masses larger than  $10^{10.2} M_\odot$ , but compact disks with  $h_R < 2$  kpc. Such galaxies are uncommon. It suggests that the galaxies selected for  $j_\star$  measurements may be biased towards compact galaxies, which may not be representative enough to draw definitive conclusions.

Moreover, the significance of rotation in disks quantified by  $\epsilon_{f_{\text{disk}}}$  here is hard to be accurately approximated in observa-

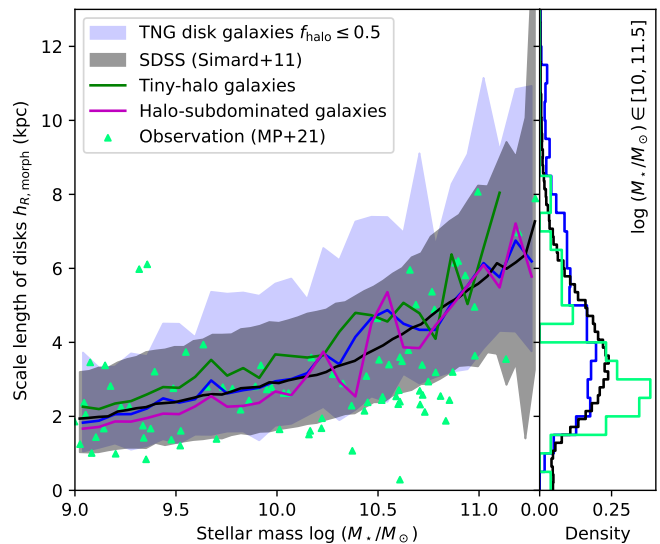


**Fig. 5.** The mass- $h_{R,\text{morph}}$  diagram. Disk galaxies from TNG50 are represented by the blue-shaded area, while observed disk galaxies from SDSS DR7 are shown in the gray-shaded region. The solid profiles are the median. The shaded areas denote the  $1\sigma$  envelope, representing the 16th and 84th percentiles. For the SDSS data, we utilized scale length values from Simard et al. (2011) and stellar mass data from Mendel et al. (2014). It is apparent that SDSS galaxies are consistent with TNG50 disk galaxies, and the difference between halo-subdominated galaxies and tiny-halo galaxies is minimal. The green triangles and the histograms on the right illustrate that the data utilized in Mancera Piña et al. (2021) (green) are biased towards smaller-sized galaxies.

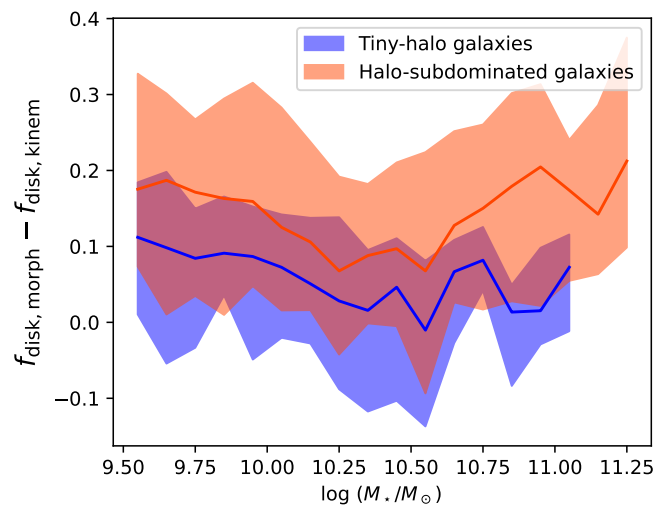


**Fig. 6.** The relative mass fraction of disk structures of tiny-halo (blue) and halo-subdominated (red) galaxies, measured by morphological  $f_{\text{disk,morph}}$  and kinematic  $f_{\text{disk,kinem}}$  methods. The morphologically defined disks are generally 10 percent larger than those defined in the kinematical method from Du et al. (2019, 2020). The envelopes of shaded regions represent the 16th and 84th percentiles and the solid profile is the median value.

tions. As shown in Figure 6, the mass fraction of morphologically decomposed disk structures  $f_{\text{disk,morph}}$  are generally slightly larger by about 0 – 0.2 (median at  $\sim 0.1$ ) in tiny-halo galaxies (blue) than those measured using the kinematical method  $f_{\text{disk,kinem}}$  from Du et al. (2019, 2020). The difference is larger

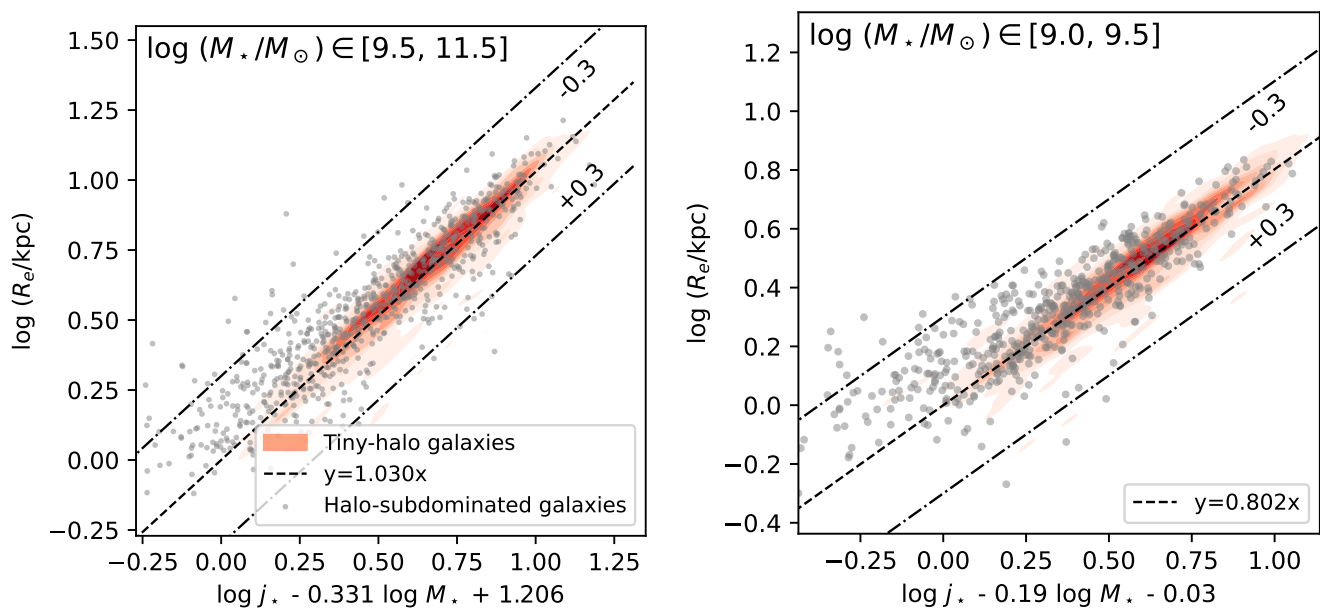


**Fig. 7.** The fiducial  $j_*$ - $M_*$ - $R_e$  relation of tiny-halo galaxies (red KDE contours) from the TNG50 simulation. This tight relation is obtained by a surface fitting of the 3D space of  $j_*$ ,  $M_*$ , and  $R_e$  using two mass ranges  $\log(M_*/M_\odot) \in [9.5, 11.5]$  and  $\in [9.0, 9.5]$ . Halo-subdominated galaxies (gray dots) are also shown for comparison.

in halo-subdominated galaxies (red) reaching about 0.05 – 0.3 (red, median at  $\sim 0.2$ ). If we take the potential overestimation of  $\epsilon f_{\text{disk}}$  from 0.5 to 0.72 in observations into account, it will lead to an offset toward the right side of the fiducial  $j_*$ - $M_*$ - $h_R$  relation about 0.15 dex. The inconsistency between Mancera Piña et al. (2021) and TNG50 is understandable.

In conclusion, we do not find any clear evidence of incorrect properties in the size and rotations of galaxies in TNG50. The inconsistency in the  $j_*$ - $M_*$ - $h_R$  relation between observations and the TNG simulations is likely attributed to several factors: (1) The substantial uncertainty in the measurement of  $j_*$ ; (2) overestimation of  $\epsilon f_{\text{disk}}$ ; (3) The limited statistical quality of the data sample; (4) The bias towards compact galaxies; (5) The contamination from halo-subdominated galaxies. This outcome may further lead to the weak dependence on  $j_*$  of the mass-size relation.

#### 4. The $j_*$ - $M_*$ - $R_e$ relation: the origin of the mass-size relation and its scatter

##### 4.1. The $j_*$ - $M_*$ - $R_e$ relation

A similar fiducial  $j_*$ - $M_*$ - $R_e$  relation can be derived, assuming that the half-mass radius of galaxy  $R_e$  is proportional to  $h_R$ . Figure 7 shows the surface fitting result of the 3D space of  $j_*$ ,  $M_*$ , and  $R_e$  using two mass ranges. The fitting result of tiny-halo galaxies with  $M_* \in [10^{9.5}, 10^{11.5}]M_\odot$  (red KDE map in the left panel of Figure 7) gives

$$\log R_e = (1.019 \pm 0.015) [\log j_* - (0.331 \pm 0.012) \log M_* + (1.206 \pm 0.093)]. \quad (8)$$

It is clear that  $R_e$  follows a very similar correlation to the fiducial  $j_*$ - $M_*$ - $h_R$  relation in Figure 4. This equation can also be written as

$$\log R_e \simeq \log j_* - 0.29 \log M_* + (1.2 - 0.04 \log M_*) \quad (9)$$

that can be directly compared with the fiducial  $j_*$ - $M_*$ - $h_R$  relation. The constant term  $1.2 - 0.04 \log(M_*/M_\odot)$  is approximately 0.8 for the sample of galaxies whose  $\log(M_*/M_\odot) \simeq 10$ . Remarkably, the tiny-halo galaxies exhibit a tight correlation between  $j_*$ - $M_*$  and galaxy size, which closely resembles the  $j_*$ - $M_*$ - $h_R$  relation. We have verified that the half-mass radius of kinematically-derived disk structures, denoted as  $R_{e,\text{disk}}$ , is 1.4–1.8 (median at  $\sim 1.6$ ) times larger than  $h_{R,\text{morph}}$  (left panel of Figure 8). This result aligns well with the expected behavior for disk structures with exponential profiles. Furthermore, the ratio between  $R_e$  and  $h_{R,\text{morph}}$   $R_e/h_{R,\text{morph}}$  varies from 0.9 to 1.5 (median at  $\sim 1.2$ ) in both TNG50 and as the scale length  $h_R$ , shown in Figure 8.

Equation (8) can also be written as  $R_e \propto \lambda M_*^{0.212}$  where the spin parameter of galaxies  $\lambda \propto \frac{j_*}{M_*^{0.543}}$  is nearly constant according to the second panel of Figure 2. It thus gives the overall mass-size relation  $R_e \propto M_*^{0.225}$  of disk galaxies with  $M_* \in [10^{9.5}, 10^{11.5}]M_\odot$  shown in the first panel of Figure 2. The large scatter originates from the scatter of  $\lambda$ . Therefore, the fiducial  $j_*$ - $M_*$ - $R_e$  relation explains well both the mass-size relation of disk galaxies and its large scatter. This result suggests that the disk structure of galaxies while displaying a broad range of sizes, does not deviate significantly from the exponential hypothesis. Stellar migration (e.g., Debattista et al. 2006; Roškar et al. 2012; Berrier & Sellwood 2015) does not dramatically alter the fiducial  $j_*$ - $M_*$ -size relation. It is also worth emphasizing that halo-subdominated galaxies (gray dots in Figure 7) adhere to a scaling relation that is nearly identical to tiny-halo galaxies, despite the large scatter. We can conclude that nature shapes the overall  $j_*$ - $M_*$  and mass-size relation. And the effect of external factors plays a minor role.



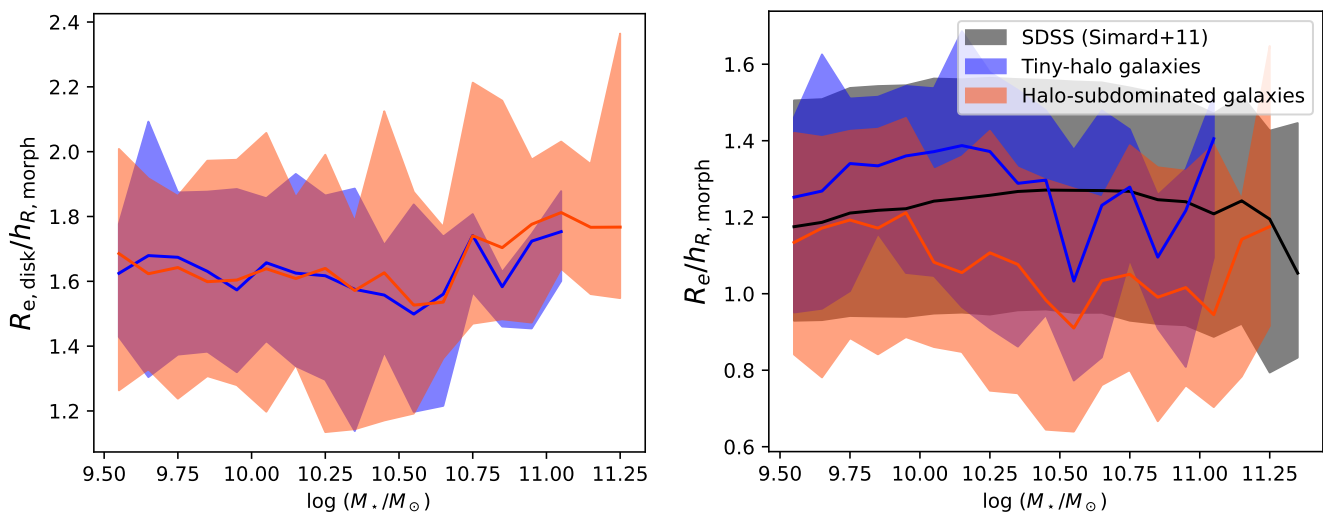


**Fig. 8.** The ratio between the effective radius ( $R_e$ ) and the morphologically measured scale length ( $h_{R,\text{morph}}$ ) as a function of stellar mass ( $M_*$ ). Here,  $R_e$  represents the half-mass radii of entire galaxies, while  $R_{e,\text{disk}}$  specifically denotes the half-mass radii of the disk structures derived through the kinematic method. Tiny-halo and halo-subdominated galaxies are shown in blue and red, respectively. The envelopes of shaded regions represent the 16th and 84th percentiles and the solid profile is the median value. The black profile shows the measurement from SDSS  $r$ -band adopted from Simard et al. (2011) for comparison.

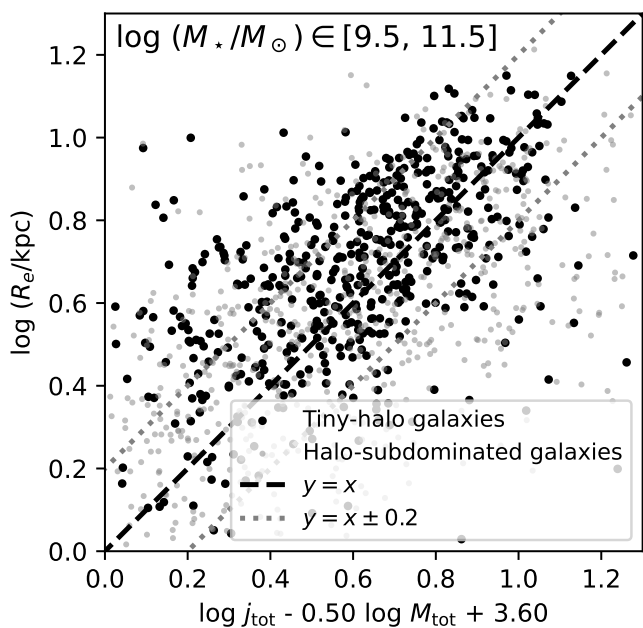


**Fig. 9.** The relation between galaxy size and dark matter halo virial radius in the TNG50 simulation. Central tiny-halo galaxies (black dots) and central halo-subdominated galaxies (gray dots) are shown here. The  $x$ -axis represents  $\lambda r_{\text{vir}}$ . This correlation is given by Equation (10) instead of running a 3D surface fitting.

#### 4.2. The relation between galaxy size and dark matter halo virial radius

We adopt  $\log j_* \simeq \log j_{\text{tot}}$  and  $\log M_* \simeq (\log M_{\text{tot}} - 4.8)/0.67$  from Du et al. (2022), then Equation (8) can be written as

$$\log R_e \simeq \log j_{\text{tot}} - 0.50 \log M_{\text{tot}} + 3.60 \quad (10)$$

Such a correlation does exist for galaxies with stellar mass  $10^{9.5} - 10^{11.5} M_\odot$  but has a quite large scatter, as shown in Figure 9. Note that we here do not run a surface fitting of  $j_{\text{tot}}$ ,  $M_{\text{tot}}$ , and  $R_e$  due to the bad statistic and large scatter. When considering  $r_{\text{vir}}/\text{kpc} \simeq 0.02(M_{\text{tot}}/M_\odot)^{1/3}$  and the constant spin parameter defined as  $\lambda_{\text{tot}} = (10^{3.60}/0.02) j_{\text{tot}}/M_{\text{tot}}^{0.81} = 0.08$  adopting  $j_{\text{tot}}/M_{\text{tot}}^{0.81} \sim 10^{-6.37}$  from Du et al. (2022, Equation 8), Equation (10) is written as

$$R_e \sim \lambda_{\text{tot}} r_{\text{vir}} \sim 0.08 r_{\text{vir}} \quad (11)$$

As a result, TNG50 predicts that the ratio of galaxy size to halo virial radius is  $R_e/r_{\text{vir}} \sim 0.08$ . This finding is in agreement with results derived from pure  $N$ -body simulations, where  $R_e \propto \lambda r_{\text{vir}}$  (Mo et al. 1998; Dalcanton et al. 1997; Somerville et al. 2008), while also considering the adjustment for the offset from  $j \propto M^{2/3}$  and the correction of the stellar-to-halo mass relation for disk galaxies. It's important to emphasize that defining  $\lambda \propto j/M^{2/3}$  in a conventional manner introduces an additional dependency on the mass. The size-size relation is very sensitive to the scaling factor of  $\log(M_{\text{tot}}/M_\odot)$ . A deviation of  $0.02 \log(M_{\text{tot}}/M_\odot)$  can lead to an uncertainty of  $R_e$  by factor 2. Additionally, we have validated that the correlation does not hold for less massive galaxies, which is consistent with the findings of Karmakar et al. (2023). The halo-subdominated galaxies (represented by gray dots) also exhibit a relatively large scatter. Hence, such a size-size correlation is not always apparent, explaining the somewhat conflicting conclusions shown in Yang et al. (2023) and Karmakar et al. (2023). Thus, we suggest the galaxy size-virial radius relation should not be viewed as conclusive evidence of whether the characteristics of galaxies are dependent on their parent dark matter halos.

## 5. Summary

In this study, we elucidate the influence of internal and external processes on the scaling relations of the specific angular momentum  $j_*$ , mass  $M_*$ , and size of galaxies from TNG50. We employ

a fully automatic kinematical method to decompose the kinematic structures of IllustrisTNG galaxies. Galaxies with more massive kinematic stellar halos generally have experienced a stronger influence from external factors, e.g., mergers or close tidal interactions with neighbor galaxies.

Our analysis verifies the crucial role played by the inherent scatter in  $j_*$  arising from internal (natural) processes including but not limited to the properties of protogalaxies, secular processes, and host dark matter halos of galaxies. We select galaxies that have tiny kinematic stellar halos of mass ratio  $f_{\text{halo}} \leq 0.2$  to isolate the effect of internal physical processes. Such galaxies populate widely over the observed  $j_*$ - $M_*$  relation and the mass-size relation in the local Universe. We confirmed that the disk structures of tiny-halo galaxies in IllustrisTNG adhere to the exponential hypothesis. The substantial scatter in the  $j_*$ - $M_*$  relation then provides a robust explanation for the fiducial  $j_*$ - $M_*$ - $h_R$  relation. It further leads to the mass-size relation and the large scatter of galaxy size. Additionally, our findings indicate that the impact of stellar migrations, as suggested by previous studies, has a minor effect on the overall properties of galaxies. The companion piece to this paper will explore the evolutionary process of galaxies of different sizes (Ma, Du, et al., in preparation).

Halo-subdominated galaxies with  $0.2 < f_{\text{halo}} \leq 0.5$  are moderately influenced by external processes. Such galaxies closely align with a scaling relation similar to that of tiny-halo galaxies, but have a large scatter and systematically offset toward the low  $j_*$  side. This result underscores the dominant role of internal factors in shaping the overall  $j_*$ - $M_*$  and mass-size relation, with external effects playing a minor role. Additionally, we examine the correlation between galaxy size and the virial radius of the dark matter halo after taking into the adjustment for the offset from  $j \propto M^{2/3}$  and the correction of the stellar-to-halo mass relation for disk galaxies. Such a correlation is likely to be unclear to make a robust conclusion.

*Acknowledgements.* The authors acknowledge the support by the Natural Science Foundation of Xiamen, China (No. 3502Z202372006), the Fundamental Research Funds for the Central Universities (No. 20720230015), the Science Fund for Creative Research Groups of the National Science Foundation of China (NSFC) (No. 12221003), and the China Manned Space Program. We also acknowledge constructive comments and suggestions from H. Mo and D.Y. Zhao. L.C.H. acknowledges the support by the NSFC grant (11721303, 11991052, 12011540375, 12233001), the National Key R&D Program of China (2022YFF0503401), and the China Manned Space Project (CMS-CSST-2021-A04, CMS-CSST-2021-A06). S.L. acknowledges the support by the NSFC grant (No. 11988101) and the K. C. Wong Education Foundation. Y.J.P. acknowledges the support by the NSFC Grant No. 12125301, 12192220, 12192222, and the science research grants from the China Manned Space Project with NO. CMS-CSST-2021-A07. The TNG50 simulation used in this work, one of the flagship runs of the IllustrisTNG project, has been run on the HazelHen Cray XC40-system at the High Performance Computing Center Stuttgart as part of project GCS-ILLU of the Gauss centers for Supercomputing (GCS). This work is also strongly supported by the Computing Center in Xi'an.

## References

Avila-Reese, V., Zavala, J., Firmani, C., & Hernández-Toledo, H. M. 2008, *AJ*, 136, 1340  
 Berrier, J. C., & Sellwood, J. A. 2015, *ApJ*, 799, 213  
 Blanton, M. R., Hogg, D. W., Bahcall, N. A., et al. 2003, *ApJ*, 594, 186  
 Bradford, J. D., Geha, M. C., & van den Bosch, F. C. 2016, *ApJ*, 832, 11  
 Covington, M., Dekel, A., Cox, T. J., Jonsson, P., & Primack, J. R. 2008, *MNRAS*, 384, 94  
 Covington, M. D., Primack, J. R., Porter, L. A., et al. 2011, *MNRAS*, 415, 3135  
 Dalcanton, J. J., Spergel, D. N., & Summers, F. J. 1997, *ApJ*, 482, 659  
 Davé, R., Anglés-Alcázar, D., Narayanan, D., et al. 2019, *MNRAS*, 486, 2827  
 Davis, M., Efstathiou, G., Frenk, C. S., & White, S. D. M. 1985, *ApJ*, 292, 371  
 Debattista, V. P., Mayer, L., Carollo, C. M., et al. 2006, *ApJ*, 645, 209

Desmond, H., Mao, Y.-Y., Wechsler, R. H., Crain, R. A., & Schaye, J. 2017, *MNRAS*, 471, L11  
 Doménech-Moral, M., Martínez-Serrano, F. J., Domínguez-Tenreiro, R., & Serna, A. 2012, *MNRAS*, 421, 2510  
 Doroshkevich, A. G. 1970, *Astrofizika*, 6, 581  
 Du, M., Ho, L. C., Debattista, V. P., et al. 2021, *ApJ*, 919, 135  
 —. 2020, *ApJ*, 895, 139  
 Du, M., Ho, L. C., Yu, H.-R., & Debattista, V. P. 2022, *ApJ*, 937, L18  
 Du, M., Ho, L. C., Zhao, D., et al. 2019, *ApJ*, 884, 129  
 Dubois, Y., Beckmann, R., Bournaud, F., et al. 2021, *A&A*, 651, A109  
 Dutton, A. A., van den Bosch, F. C., Dekel, A., & Courteau, S. 2007, *ApJ*, 654, 27  
 Fall, S. M. 1983, in *Internal Kinematics and Dynamics of Galaxies*, ed. E. Athanassoula, Vol. 100, 391–398  
 Fall, S. M., & Efstathiou, G. 1980, *MNRAS*, 193, 189  
 Fall, S. M., & Rodríguez-Gomez, V. 2023, *ApJ*, 949, L14  
 Fernández Lorenzo, M., Sulentic, J., Verdes-Montenegro, L., & Argudo-Fernández, M. 2013, *MNRAS*, 434, 325  
 Fisher, D. B., & Drory, N. 2008, *AJ*, 136, 773  
 Genel, S., Nelson, D., Pillepich, A., et al. 2018, *MNRAS*, 474, 3976  
 Grand, R. J. J., Gómez, F. A., Marinacci, F., et al. 2017, *MNRAS*, 467, 179  
 Gurovich, S., Freeman, K., Jerjen, H., Staveley-Smith, L., & Puerari, I. 2010, *AJ*, 140, 663  
 Herpich, J., Stinson, G. S., Dutton, A. A., et al. 2015, *MNRAS*, 448, L99  
 Hopkins, P. F., Lauer, T. R., Cox, T. J., Hernquist, L., & Kormendy, J. 2009, *ApJS*, 181, 486  
 Hoyle, F. 1951, in *Problems of Cosmical Aerodynamics*, 195  
 Huertas-Company, M., Rodríguez-Gomez, V., Nelson, D., et al. 2019, *MNRAS*, 489, 1859  
 Jiang, F., Dekel, A., Kneller, O., et al. 2019, *MNRAS*, 488, 4801  
 Karmakar, T., Genel, S., & Somerville, R. S. 2023, *MNRAS*, 520, 1630  
 Kroupa, P., Aarseth, S., & Hurley, J. 2001, *MNRAS*, 321, 699  
 Lagos, C. d. P., Theuns, T., Stevens, A. R. H., et al. 2017, *MNRAS*, 464, 3850  
 Lange, R., Driver, S. P., Robotham, A. S. G., et al. 2015, *MNRAS*, 447, 2603  
 Lelli, F., McGaugh, S. S., & Schombert, J. M. 2016, *ApJ*, 816, L14  
 Lelli, F., McGaugh, S. S., Schombert, J. M., Desmond, H., & Katz, H. 2019, *MNRAS*, 484, 3267  
 Liao, S., Gao, L., Frenk, C. S., et al. 2019, *MNRAS*, 490, 5182  
 Mancera Piña, P. E., Posti, L., Fraternali, F., Adams, E. A. K., & Oosterloo, T. 2021, *A&A*, 647, A76  
 Marinacci, F., Vogelsberger, M., Pakmor, R., et al. 2018, *MNRAS*, 480, 5113  
 Mendel, J. T., Simard, L., Palmer, M., Ellison, S. L., & Patton, D. R. 2014, *ApJS*, 210, 3  
 Minchev, I., Famaey, B., Quillen, A. C., et al. 2012, *A&A*, 548, A127  
 Mo, H. J., Mao, S., & White, S. D. M. 1998, *MNRAS*, 295, 319  
 Muñoz-Mateos, J. C., Sheth, K., Regan, M., et al. 2015, *ApJS*, 219, 3  
 Naab, T., Johansson, P. H., & Ostriker, J. P. 2009, *ApJ*, 699, L178  
 Naab, T., & Ostriker, J. P. 2017, *ARA&A*, 55, 59  
 Naiman, J. P., Pillepich, A., Springel, V., et al. 2018, *MNRAS*, 477, 1206  
 Nelson, D., Pillepich, A., Springel, V., et al. 2018, *MNRAS*, 475, 624  
 Nelson, D., Springel, V., Pillepich, A., et al. 2019, *Computational Astrophysics and Cosmology*, 6, 2  
 Noordermeer, E., & Verheijen, M. A. W. 2007, *MNRAS*, 381, 1463  
 Obreja, A., Macciò, A. V., Moster, B., et al. 2018, *MNRAS*, 477, 4915  
 Obreschkow, D., & Glazebrook, K. 2014, *ApJ*, 784, 26  
 Oser, L., Naab, T., Ostriker, J. P., & Johansson, P. H. 2012, *ApJ*, 744, 63  
 Pakmor, R., Bauer, A., & Springel, V. 2011, *MNRAS*, 418, 1392  
 Pakmor, R., Springel, V., Bauer, A., et al. 2016, *MNRAS*, 455, 1134  
 Papastergis, E., Adams, E. A. K., & van der Hulst, J. M. 2016, *A&A*, 593, A39  
 Peebles, P. J. E. 1969, *ApJ*, 155, 393  
 Pillepich, A., Springel, V., Nelson, D., et al. 2018, *MNRAS*, 473, 4077  
 Pillepich, A., Nelson, D., Springel, V., et al. 2019, *MNRAS*, 490, 3196  
 Porter, L. A., Somerville, R. S., Primack, J. R., et al. 2014, *MNRAS*, 445, 3092  
 Proctor, K. L., Lagos, C. d. P., Ludlow, A. D., & Robotham, A. S. G. 2024, *MNRAS*, 527, 2624  
 Rodríguez-Gomez, V., Genel, S., Vogelsberger, M., et al. 2015, *MNRAS*, 449, 49  
 Rodríguez-Gomez, V., Snyder, G. F., Lotz, J. M., et al. 2019, *MNRAS*, 483, 4140  
 Rodríguez-Gomez, V., Genel, S., Fall, S. M., et al. 2022, *MNRAS*, 512, 5978  
 Romanowsky, A. J., & Fall, S. M. 2012, *ApJS*, 203, 17  
 Roškar, R., Debattista, V. P., Quinn, T. R., Stinson, G. S., & Wadsley, J. 2008, *ApJ*, 684, L79  
 Roškar, R., Debattista, V. P., Quinn, T. R., & Wadsley, J. 2012, *MNRAS*, 426, 2089  
 Schaye, J., Crain, R. A., Bower, R. G., et al. 2015, *MNRAS*, 446, 521  
 Sellwood, J. A. 2014, *Reviews of Modern Physics*, 86, 1  
 Shankar, F., Marulli, F., Bernardi, M., et al. 2013, *MNRAS*, 428, 109  
 Shen, S., Mo, H. J., White, S. D. M., et al. 2003, *MNRAS*, 343, 978  
 Simard, L., Mendel, J. T., Patton, D. R., Ellison, S. L., & McConnachie, A. W. 2011, *ApJS*, 196, 11

- Somerville, R. S., & Davé, R. 2015, *ARA&A*, 53, 51  
Somerville, R. S., Barden, M., Rix, H.-W., et al. 2008, *ApJ*, 672, 776  
Springel, V. 2010, *MNRAS*, 401, 791  
Springel, V., White, S. D. M., Tormen, G., & Kauffmann, G. 2001, *MNRAS*, 328, 726  
Springel, V., Pakmor, R., Pillepich, A., et al. 2018, *MNRAS*, 475, 676  
Sweet, S. M., Fisher, D., Glazebrook, K., et al. 2018, *ApJ*, 860, 37  
Teklu, A. F., Remus, R.-S., Dolag, K., et al. 2015, *ApJ*, 812, 29  
Weinberger, R., Springel, V., Hernquist, L., et al. 2017, *MNRAS*, 465, 3291  
White, S. D. M. 1984, *ApJ*, 286, 38  
White, S. D. M., & Rees, M. J. 1978, *MNRAS*, 183, 341  
Yang, H., Gao, L., Frenk, C. S., et al. 2023, *MNRAS*, 518, 5253  
Zana, T., Lupi, A., Bonetti, M., et al. 2022, *MNRAS*, 515, 1524  
Zanisi, L., Shankar, F., Lapi, A., et al. 2020, *MNRAS*, 492, 1671  
Zaritsky, D., Courtois, H., Muñoz-Mateos, J.-C., et al. 2014, *AJ*, 147, 134  
Zavala, J., Frenk, C. S., Bower, R., et al. 2016, *MNRAS*, 460, 4466  
Zjupa, J., & Springel, V. 2017, *MNRAS*, 466, 1625